magnetism

MDPI

Supplementary material to the article

Phase Diagram Mapping out the Complex Magnetic Structure of Single Crystals of (Gd, Er)B_4 Solid Solutions

Sueli H. Masunaga [1,2,*], Vagner B. Barbeta [1], Fábio Abud [2,3], Milton S. Torikachvili [4] and Renato F. Jardim [2]

[1] Departamento de Física, Centro Universitário FEI, São Bernardo do Campo 09850-901, SP, Brazil; vbarbeta@fei.edu.br
[2] Instituto de Física, Universidade de São Paulo, São Paulo 05315-970, SP, Brazil; fabio.abud@usp.br (F.A.); rjardim@if.usp.br (R.F.J.)
[3] Departamento de Engenharia de Materiais, Escola de Engenharia de Lorena, Universidade de São Paulo, Lorena 12612-550, SP, Brazil
[4] Department of Physics, San Diego State University, San Diego, CA 92182, USA; miltont@sdsu.edu
* Correspondence: sueli.masunaga@gmail.com

1. $Gd_{1-x}Er_xB_4$ single crystals

The Laue photographs shown in Reference [1] (Ref. [25] in the original manuscript) revealed the absence of distortions, asterisms, or smearing in the diffraction spots, indicative of a high degree of crystallinity in the single-crystal samples of $Gd_{1-x}Er_xB_4$. Furthermore, we conducted an analysis of crystal orientation, which revealed that the larger facets of single crystals of $Gd_{1-x}Er_xB_4$ (x = 0.2 and 0.4) are perpendicular to the c-axis.

The formation of solid solutions of $Gd_{1-x}Er_xB_4$ with nominal compositions x = 0.2 and 0.4 was verified in a prior study wherein the results of X-ray diffraction (XRD) and temperature-dependent magnetic susceptibility [$\chi(T)$] analyses were precisely evaluated. As observed in Figure 5 and Table 1 of Reference [1], a systematic shift in the (001) reflection towards higher 2θ values and a concomitant decrease in the lattice parameters throughout the series were observed with increasing Er content, providing evidence for the establishment of solid solutions. The effective magnetic moment (μ_{eff}) values, derived from $\chi(T)$ data and analyzed using the Curie–Weiss law, exhibited consistency with the calculated μ_{eff} values for Gd^{3+} and Er^{3+} free ions, as shown in Table 2 of Reference [1]. All these experimental findings further support the effective partial substitution of Er for Gd within this series.

1. Magnetization data

The DC magnetization measurements were taken in a commercial system (Quantum Design's PPMS, model Dynacool). The DC magnetization data were acquired using a vibrating sample magnetometer (VSM), an option in the PPMS. Properly oriented crystals were attached to a sample holder using DUCO cement and measured using the protocols described below.

Isothermal magnetization ($M \times H$) data were acquired by cooling the samples in zero applied field to the target temperature. Following temperature stabilization, magnetization curves were obtained by sweeping the applied magnetic field from zero to +9 T, then from +9 T to –9 T, and finally from –9 T to +9T. These curves are shown in

Figures S1 and S2. The first quadrant, measured from zero to +9 T, has been omitted for clarity.

Temperature-dependent magnetization curves ($M \times T$) were acquired by employing zero field cooling (ZFC) and field cooling (FC) procedures. Initially, the sample was cooled down to 2 K in the absence of an applied magnetic field. Subsequently, the desired magnetic field was set at 2 K, and the ZFC curve was measured from 2 K up to 300 K. Finally, the FC curve was measured from 300 K to 2 K under the same applied magnetic field. The ZFC and FC curves are displayed in Figures S3 and S4.

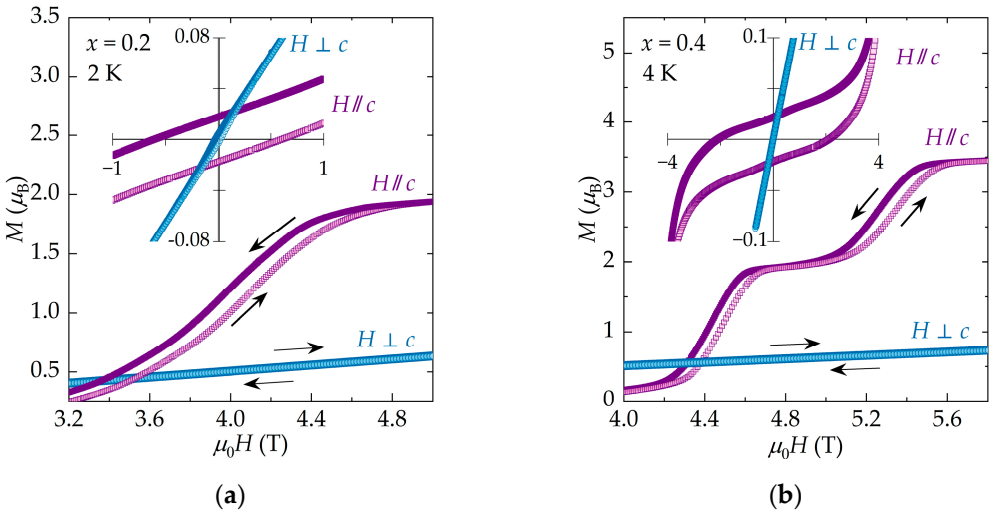

(**a**) (**b**)

Figure S1. $M \times H$ curves under $H \parallel c$ and $H \perp c$ for single crystals of $Gd_{1-x}Er_xB_4$ with (**a**) $x = 0.2$ at $T = 2$ K; (**b**) $x = 0.4$ at $T = 4$ K. The arrows indicate the sweeping direction of the applied magnetic field. The insets show an expanded view of the low-field limits of the curves.

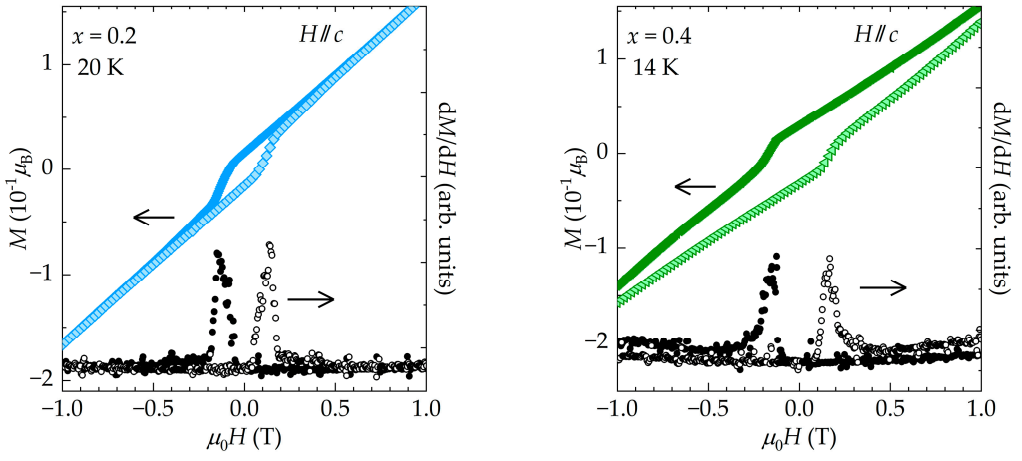

(**a**) (**b**)

Figure S2. $M \times H$ under $H \parallel c$ for single crystals of $Gd_{1-x}Er_xB_4$ with (**a**) $x = 0.2$ at $T = 20$ K; (**b**) $x = 0.4$ at $T = 14$ K. The corresponding derivatives, dM/dH, for both compositions are presented at the bottom of the plots.

Figure S1 shows an expanded view of the $M \times H$ curves in the region where magnetic transitions induced by a magnetic field occur. In the case of the $Gd_{0.8}Er_{0.2}B_4$ single crystal, only one metamagnetic transition of the Er^{3+} ions occur. On the other hand, in the $Gd_{0.6}Er_{0.4}B_4$ single crystal, two successive metamagnetic transitions take place, with a magnetization plateau at ½ M_S being clearly observable.

Single crystals of $Gd_{1-x}Er_xB_4$ (x = 0.2 and 0.4) exhibit pronounced magnetic anisotropy along the c-axis, as shown in the insets of Figure S1. In the case of x = 0.2, the coercive field μ_0H_C ~ 0.60 T along the c-axis is ~ 21 times larger than the observed value along the perpendicular direction. In the x = 0.4 sample, the magnetic anisotropy is even more pronounced, with μ_0H_C ~ 2.1 T along the c-axis and negligible coercivity along the ab-plane.

Figure S2 shows an expanded view of the $M \times H$ and dM/dH curves near zero applied magnetic field, acquired at 20 K and 14 K for samples with x = 0.2 and 0.4, respectively. The discernible features in dM/dH result from variations in the slopes of the $M \times H$ curves, attributable to the occurrence of remanent magnetization and the coercive field within the magnetic hysteresis loops.

Figure S3 shows $M/H \times T$ curves for samples with x = 0.2 and 0.4, obtained through ZFC and FC processes. Along the c-axis, irreversibility between the ZFC and FC curves manifests below the Néel transition temperature of the $Gd_{1-x}Er_xB_4$ (x = 0.2 and 0.4) samples. Conversely, for both samples, irreversibility extends to higher temperatures, accompanied by the appearance of remnant magnetization along the ab-plane. The observed irreversibility decreases considerably with increasing applied magnetic field, as evidenced by the evolution of the ZFC/FC curves with increasing magnetic field strength, as seen in Figure S3.

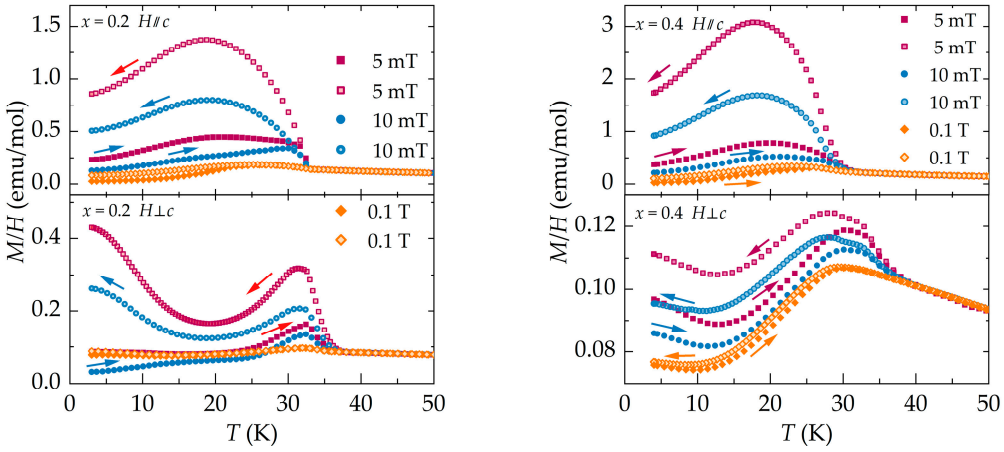

(**a**) (**b**)

Figure S3. $M/H \times T$ for $Gd_{1-x}Er_xB_4$ samples with (**a**) x = 0.2 and (**b**) x = 0.4 measured under magnetic fields up to 0.1 T. The closed symbols represent zero-field-cooled (ZFC) curves, while the open symbols depict field-cooled (FC) curves, as indicated by the arrows.

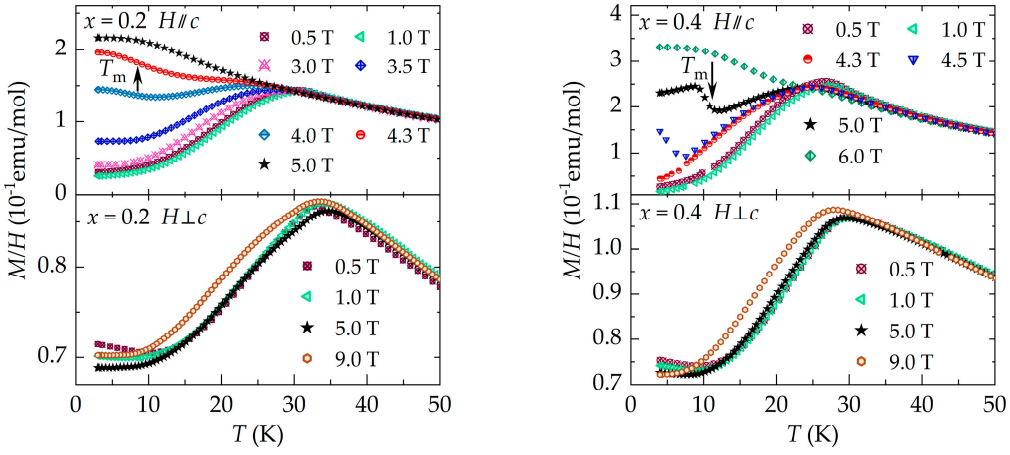

(**a**) (**b**)

Figure S4. $M/H \times T$ for $Gd_{1-x}Er_xB_4$ samples with (**a**) $x = 0.2$ and (**b**) $x = 0.4$ measured under magnetic fields ranging from 0.5 T to 9.0 T in the FC process. The shallow maxima observed at T_m in the $C_p(T)$ curves correspond to the inflexion points in the $M/H \times T$ curves (marked by the arrows in the figure).

Figure S4 displays the evolution of FC curves taken under various applied magnetic fields ranging from 0.5 T to 9 T. Along the direction perpendicular to the *c*-axis and for both samples with $x = 0.2$ and 0.4, the $M/H \times T$ curves exhibit features characteristic of antiferromagnetic AF systems. However, changes in the AF characteristics are evident in the curves taken above 3.5 T and 4.3 T, corresponding to the metamagnetic transitions observed in the $M \times H$ curves for samples with $x = 0.2$ and 0.4, respectively. In addition, the magnitude of $M/H \times T$ is slightly greater for the $x = 0.4$ samples, as illustrated in Figure S4. Such a difference in the magnitude of the magnetic moments is consistent with the higher effective magnetic moment of Er^{3+} (9.59 μ_B) in comparison with Gd^{3+} (7.94 μ_B).

References

1. Masunaga, S.H.; Barbeta, V.B.; Abud, F.; Torikachvili, M.S.; Jardim, R.F. Anomalous Ferromagnetic Phase in the $Gd_{1-x}Er_xB_4$ Series: Crystal Growth, Thermal, and Magnetic Properties. *Crystals* **2023**, *13*, 1137, doi:10.3390/cryst13071137.